Predicting the Effect of Dopants on CO_2 Adsorption on Transition Metal Carbides: Case Study on TiC (001)

Martí López,[†] Francesc Viñes[*,†] Michael Nolan,[*,‡] and Francesc Illas[,†]

[†] *Departament de Ciència de Materials i Química Física & Institut de Química Teòrica i Computacional (IQTCUB), Universitat de Barcelona, c/ Martí i Franqués 1-11, Barcelona 08028, Spain.*

[‡] *Tyndall National Institute, Lee Maltings, University College Cork, Cork T12R5CP, Ireland.*

*Corresponding authors: francesc.vines@ub.edu, michael.nolan@tyndall.ie

Abstract

Previous work has shown that doping the TiC (001) surface with early transition metals significantly affects CO_2 adsorption and activation which opens a possible way to control this interesting chemistry. In this work we explore other possibilities which include non-transition metals elements (Mg, Ca, Sr, Al, Ga, In, Si, Sn) as well as late transition metals (Pd, Pt, Rh, Ir) and lanthanides (La, Ce) often used in catalysis. Using periodic slab models with large supercells and state-of-the-art density functional theory (DFT) based calculations, we show that, in all the studied cases, CO_2 appears as bent and, hence, activated. However, the effect is especially pronounced for dopants with large ionic crystal radii. These can increase desorption temperature by up to 230 K, almost twice the value predicted when early transition metals are used as dopants. However, a detailed analysis of the results shows that the main effect does not come from electronic structure perturbations but from the distortion that the dopant generates into the surface atomic structure. A simple descriptor is proposed that would allow predicting the effect of the dopant on the CO_2 adsorption energy in transition metal carbide surfaces without requiring DFT calculations.

1. Introduction

Finding ways to mitigate global warming, which is primarily driven by the increase in the concentration of CO_2 in the Earth's atmosphere as a result of the use of fossil fuels, has become a major research topic. Global warming is predicted to trigger harmful consequences such as the ocean acidification,[1] increases in sea level,[2] or increasing temperatures through the cycle-carbon feedback.[3] Finding alternative, environmentally friendly energy sources to ensure a sustainable industry has become a hugely significant.[4-6] However, although many successes have been achieved, the increasing energy demand and the concomitant technical complexity makes the translation of such advances into real alternatives to finally overcome the fossil fuel energy dependence, in the short-to-medium term, difficult to achieve.

Meanwhile, new strategies are being explored to address the more immediate issues. In particular, CO_2 capture and storage (CCS),[7-9] and usage (CCU)[10] technologies are being actively investigated. Several CCS approaches are currently being explored with absorption constituting the dominant technology, although adsorption or membrane gas separation are other possibilities, which are in a developmental research stage.[8,9,11,12] To move forwards by adding extra value to the captured CO_2, CCU technology is slowly growing due to its important industrial and economic potential.[10] Reintroducing CO_2 to the industrial cycle through industrial processes including hydrogenation to methanol or the reverse water gas shift (RWGS) reaction would be extremely positive both for the environment as for the industry.

With CCU in mind, several materials have been tested and Ni, Pd, or Pt nanoparticles supported on oxides or sulphides[13] are the current industry choice, and have seen significant efforts to find an appropriate oxide-support. It is also worth mentioning rather recent experiments on model systems which find that small Au, Cu, and Ni nanoparticles supported on TiC (001) exhibit improved performance in methanol synthesis compared to a model of the conventional Cu/ZnO catalyst.[14,15] In addition, bare transition metal carbides such as MoC and Mo_2C have been found to be active in catalysed CO_2 activation[16] and conversion as well,[17] being highly appealing as one surpasses the handicap of using scarce and expensive late transition metals.

Indeed, computational studies, carried out in the framework of density functional theory (DFT), have shown that early transition metal carbides (TMCs) such as TiC, ZrC, WC, NbC, TaC, and, δ-MoC are able to strongly trap and activate CO_2.[18] Besides, there is experimental and/or computational evidence that δ-MoC, β-Mo_2C, WC, and NbC (001) surfaces present a

high selectivity towards CO_2 conversion to CO,[16,19,20] a component of synthesis gas used in many industrial reactions. It is also worth noticing that model catalysts joining late transition metals with TMCs are also attractive, *e.g.* Pt/Mo_2C exhibits high performance towards water gas shift (WGS) with high rates when compared to the widely used Pt/CeO_2 or Pt/TiO_2 catalysts.[21] In conclusion, TMCs bring together three key properties that confers them with significant potential for CCU applications, namely high CO_2 adsorption capability, competitive performance in catalysis, and attractive cost.

To further enhance the catalytic activity of TMCs, it has been proposed to make use of doping,[22] a strategy already successfully followed to enhance the catalytic performance of metal oxides.[23,24] In particular, the effect of doping on the TiC (001) surface with early transition metals (Hf, Ta, Zr, Nb, W, Cr, Mo, V) was systematically explored by means of DFT calculations on a series of models where the dopant substituted a Ti atom at the surface atomic layer.[22] Such calculations revealed that the effect was highly local with a strong preference for surface substitution and that the adsorption energy could be enhanced or reduced depending on whether the dopant was chosen down a group or going along a *d* series. In addition, a relationship between the calculated net charge in the doping metal atom directly interacting with CO_2 and the corresponding adsorption energy was found, indicating a significant chemical effect. To reach a more complete understanding on this issue and broaden the tuning capabilities well beyond the limited region of early transition metals, we consider in this work the effect of other dopants including *s* block alkaline earth (Mg, Ca, Sr), *p* block groups XIII (Al, Ga, In) and XIV (Si, Sn) elements, plus some extra late *d* block transition metals (Pd, Pt, Rh, Ir), even *f* elements such as lanthanides (La, Ce), with the main aim to further assess the capabilities of modified TMCs for use in CCS and CCU technologies.

2. Surface Models and Computational Details

We employ as the dopant host the widely studied TiC (001) surface, as used in an earlier work.[22] The corresponding doped models and their interaction with CO_2 have been studied in the framework of DFT with calculations carried out with the broadly used Perdew–Burke–Ernzerhof (PBE) exchange–correlation functional,[25] which is among the best functionals to describe bulk and surface properties of TMCs,[26,27] including elastic and compressive properties,[28] and significantly improving earlier descriptions[29] based on other generalized gradient functionals such as the Perdew-Wang 91 (PW91)[30] or the revised PBE (RPBE).[31] The

PBE functional, including a suitable treatment of dispersive forces, has been found to be accurate to assess the experimental interaction of CO_2 with diverse TMCs.[17,32] However, in the present work, it was found convenient to neglect the dispersion contribution to the adsorption energy because our previous studies on bare or doped TiC have shown that the main effect of dispersion is a nearly constant increase of *ca.* -0.26 eV in all calculated adsorption energies, with negligible effects on the CO_2 adsorption strength which arises primarily from the formation of C-C covalent bonds, a substrate→CO_2 charge transfer, and the $CO_2^{\delta-}$ Coulombic stabilization with TMC positively charged metal atoms, rather than any dispersion interactions. In addition, the effects of dispersion are also not significant when analysing the trends across the different dopants.[16,18,22] Nevertheless, one should always keep in mind that dispersive forces may play a role in the prediction of quantitative interaction energies,[33] and that this can have some effect on the calculated desorption rates and temperature desorption, as discussed in detail in our results.

The TiC (001) surface is represented by a periodic $(3\sqrt{2}\times3\sqrt{2})R45°$ supercell slab model consisting of six stoichiometric atomic layers periodic in surface directions with eight C and Ti atoms per layer. To provide an adequate description of the surface relaxations, the four uppermost layers were fully allowed to relax during optimizations with the two bottommost layers fixed to the pristine TiC bulk structure. To avoid the interaction between the periodically repeated slabs in the direction perpendicular to the surface, a vacuum width of 15 Å along the vacuum direction has been added.

Doping has been simulated by substituting one surface Ti atom by the corresponding dopant, a choice which is justified by previous work indicating that surface doping was always preferred,[22] and that subsurface doping has no effect on the CO_2 adsorption properties. Indeed, explicit calculations for subsurface doping further confirm this prediction, systematically finding that surface doping is the most favourable case, see Table 1. This is not surprising as surface doping allows a lower energy cost for structural relaxation to adapt to the different atomic size of the dopant compared to Ti. The dopant concentration in the different models is 3.125 at. % which is a common value in doped metal oxides, and low enough so as to neglect distortions in the TiC host, see below.

All structural optimizations have started from the bare TiC optimized geometry as in previous work.[22] The molecular structure and energy of the CO_2 molecule in the gas phase and the energy of the isolated metal atoms have been obtained by placing them in an asymmetric box 9×10×11 Å to force correct molecular orbital occupation. For the isolated metal atoms,

spin-polarized calculations have been performed to properly describe their open shell nature. The interaction of CO_2 with the different surface models starts by placing the molecule 2 Å away from the surface and exploring all possible surface sites and bonding modes as done in an earlier studiy.[22]

The CO_2 adsorption energy, E_{ads}, has been calculated as in Eq. (1)

$$E_{ads} = E_{CO_2/slab} - (E_{slab} + E_{CO_2}) \quad (1),$$

where $E_{CO_2/slab}$ is the energy of CO_2 adsorbed on the slab surface, E_{slab} is the energy of the pristine relaxed TiC slab surface model, and E_{CO_2} is the energy of isolated gas phase CO_2. Within this notation, the more negative the E_{ads} value, the stronger the interaction. For the most stable situations of the adsorbed molecule, net charges were estimated by the Bader atoms-in-molecules analysis of the total electron density.[34]

All calculations employ periodic models and have been carried out by means of the Vienna *ab initio* simulation package (VASP) code[35] which uses a plane wave basis set to expand the valence electron density,[36] and includes the effect of the atomic cores on the valence electron density by means of the by Kresse and Joubert[37] implementation of the projector augmented wave (PAW) approach of Blöchl.[38] In all cases the core electron PAWs are the ones recommended by default by the VASP developers. More details are provided at the Supporting Information (SI).

An optimized cut-off kinetic energy of 450 eV has been used for the plane-wave basis set expansion and a Monkhorst–Pack[39] grid of (2×2×1) special **k**-point was used to carry out the necessary numerical integration in the reciprocal space, so as to ensure adsorption energies to be converged below the chemical accuracy of ~0.04 eV In the case of isolated atoms or the CO2 molecule, the optimizations were carried out at **Γ** point. The structure optimization has been carried out until forces on all atoms are smaller than 0.02 eV $Å^{-1}$. The threshold convergence for the electronic energy was set to 10^{-5} eV. To speed up convergence of the calculations, a Gaussian smearing with a width of 0.2 eV has been used and the final energies are obtained by removing the smearing, *i.e.* by extrapolating to 0 K. In the case of isolated atoms or molecules, the smearing was reduced to 0.001 eV to ensure proper orbital occupation.

3. Results and Discussion

We start this section by considering several features of the doped surfaces including the ionic crystal radius of the dopant, the distance between the dopant and its neighbouring atoms, and the relative stability of the doping. The latter is defined as

$$\Delta E_{dop} = (E_{TiMC} + E_{Ti}) - (E_{TiC} + E_M) \quad (2),$$

where E_{TiMC} is the energy of the doped slab; E_{Ti} is the energy of a single Ti atom in vacuum; E_{TiC} is the energy of the pristine slab surface model; and E_M the energy of the dopant atom in vacuum. Within this notation, negative E_{dop} values indicate a favourable substitution of a single Ti atom by the doping M atom, having atomic reservoirs of both in the vacuum. Notice that this is a practical and direct way of qualitatively assessing the relative stabilities of dopants, but results in large the ΔE_{dop} values, for example as compared to using other condensed doping reservoir sources.

Thus, results in Table 1 show that the substitution of Ti with the dopants is apparently not very thermodynamically favourable, which is not surprising because mixed transition metal carbides are scarce although they do exist.[40] However, this is not so important since experimental processes for preparing doped carbides will follow other already well-established routes widely used for doping of metal oxides. The ΔE_{dop} values when allowing cell relaxation along the surface directions, ΔE_{dop}^{relax}, change by only *ca.* ~0.25 eV on average (see Table 1), reflecting the small impact of the doping agent on the TiC host crystal structure. The ΔE_{dop} results highlight that it is somewhat more favourable to dope with late transition metals or even lanthanides, rather than with *p* block elements or alkaline earth metals.

Note also that the oxidation state of the dopant reported in Table 1 has been chosen so as to correspond to the most common one. Covalent and ionic crystal atomic radius have been explored due to the mixed character of the M – C bond.[41] An initial analysis of the results in Table 1 indicates that the distortion in the C to M dopant atom follows the ionic crystal radii, as expected. Si appears to be an exception which may indicate some inaccuracy on the estimate of the ionic radius of this element or that the reported ionic radius is not adequate for comparison purposes here.

To get additional information about the effects introduced by the dopant we analyse the net charges on these atoms obtained from computed Bader's charges.[34] Table 2 shows that, in all cases, the dopant atom is partially oxidized, as expected from the rather ionic character of the TiC host.[42] Nevertheless, some differences and trends are clear. For instance, the charge on the dopant in a given group decreases along the group, being larger for the lighter atoms such

as Mg, Al, or Si. For these three elements actually, we employed different pseudopotentials with extra core electrons treated in the shell valence electron density to avoid possible artefacts produced by the default recommended pseudopotentials, which have only two, three, and four valence electrons for these elements, respectively. In any case, Table 2 values provide a first qualitative guide to focus on the trends. For all other dopants, the net charge on the dopant is smaller than the charge corresponding to Ti in the host crystal, which is likely to have an effect on the interaction of the doped surface with CO_2.

The study of CO_2 adsorption on the different doped TiC (001) surfaces follows the approach used in previous work.[22] Thus, three different adsorption modes are tested and these are: TopC, TopC-A, and MMC, as indicated in Figure 1. The TopC and TopC-A modes are equivalent, except for the relative position of the dopant. In the TopC mode one oxygen from the CO_2 is directly bonded to the dopant. Note also that in the MMC mode, the CO_2 plane is slightly bent towards the surface. The summary of results in Table 3 clearly shows that, in all cases, the CO_2 molecular angle deviates considerably from linearity. In addition, the C-O distances in the adsorbed CO_2 elongate from 1.20 Å in free CO_2 to between 1.43 and 1.52 Å. These geometrical changes are a clear sign of charge transfer from the substrate to the adsorbed molecule; a feature that is confirmed by the calculated Bader charges. In fact, upon adsorption, the CO_2 becomes negatively charged, the total net charge in the adsorbate going from -0.76 and -1.28 *e*. Moreover, the cases where the presence of the dopant leads to a large charge transfer are also those where the adsorption energy is particularly large.

Not surprisingly, the preferred adsorption mode depends on the nature of each dopant as illustrated in the SI. This can be easily explained, as the TopC-A mode will be favoured when the interaction between O atoms in CO_2 and the surface dopant atom is stronger than with surface Ti atoms. Therefore, it is logical to expect some correlation between the net charge on the dopant and the adsorption energy. The plot of the E_{ads} *vs.* q^{dop} results in a very poor correlation (not shown). However, an improved correlation is found when plotting E_{ads} versus the difference in the net charge of the C atoms in the surface plane surrounding the dopant atom, see Figure 2, and values listed in Table 2. This correlation is more useful since a C-C bond involving a carbon neighbouring the surface dopant is formed upon CO_2 adsorption, and the incorporation of the dopant into TiC directly affects the charges on the C atoms neighbouring the metal site. In fact, the plot in Figure 2 shows that the adsorption energy is related to the charge distribution. The larger the charge on the surface C atoms in the doped system relative to the same quantity for the undoped TiC (001) surface, the larger the adsorption

energy. Note, however, that Figure 2 only provides a trend which shows that, although the electrostatic interactions dominate the differences between the doped systems, they do not fully account for these differences. This implies that some chemical effects are also present.

To further investigate the role of the dopants on modifying the adsorption features of CO_2 on TiC (001) we analyse the influence of the atomic size. The rationale here is that substituting dopants on a Ti site can induce significant distortions to the surface atomic structure and the extent of the distortion largely depends on the dopant ionic radius. However, a simple plot of E_{ads} *versus* the dopant radius, and by that using the R_{dop} values encompassed in Table 1, leads again to a very poor correlation. The correlation actually becomes much better when considering instead the *geometrical distortions* caused by the dopant, which also depend on the difference in atomic size. To this end, we define ΔR as

$$\Delta R = \left| R_{dop}^{M} - R_{dop}^{Ti} \right| \quad (4),$$

where R_{dop}^{M} is the ionic crystal radius of the dopant, whereas R_{dop}^{Ti} is that corresponding for Ti, both taken from Table 1. Doping involves distortions in the surface plane of TiC, both of the convex or concave type. Therefore, it is advisable to consider the effect of the distortions in absolute value when analysing its effect on the adsorption energy. The plot of E_{ads} *vs.* ΔR is shown in Figure 3. The left panel of Figure 3 shows a clear trend, yet not really quantitative, as, interestingly, Si and In appear as clear outliers.

To try to understand the origin of this discrepancy we inspected the structure of both doped surfaces. In the case of Si, it appears that the angle between the surface C and Si atoms, and the C from CO_2 is *ca.* 114º while in the other cases, as well as in the undoped TiC (001) surface it is significantly smaller, 90º or less. This is understandable from the well-known trend of Si to prefer tetrahedral coordination and represents a clear chemical difference with respect to the rest of considered dopants. The case of In can also be understood, as the net charge in In for the doped carbide is significantly smaller than its formal oxidation number and, hence, the ionic radius does not represent the real size of this element in the doped TiC surface.

Removing the data for Si and In leads to a largely improved correlation as shown in Figure 3. This result is important because it allows one to make a reasonable estimate of the effect of a given dopant based on an intrinsic property of that dopant without needing to perform any DFT calculations, and thus can be used for a systematic screening of the effect of possible dopants towards CO_2 adsorption.

To further validate the validity of ΔR as a descriptor of CO_2 adsorption and activation, the results from the early transition metals studied in a previous work using an identical computational setup were added in Figure 3.[22] Taking into account the empirical character of the ionic crystal radii used, *cf.* Table 1, the existence of the correlation between E_{ads} and ΔR is remarkable, providing a useful descriptor for a fast exploration of the effect of a possible dopant. The correlation has been deduced for TiC (001), yet it is likely that a similar relationship exists for other transition metal carbides.

To further assess the effect of the dopant on the potential for CCS, we used transition state theory (TST) to derive the CO_2 desorption rates for each one of the doped TiC surfaces and the Hertz–Knudsen equation to estimate the corresponding adsorption rate; further details can be found in Ref. 18. Both adsorption and desorption rates depend on the working temperature, and the temperature at which both processes become equal, T_{eq}, defines the frontier between the two regimes. The variation of both rates with temperature is reported in Figure 4 for each of the explored materials using a typical partial pressure of atmospheric CO_2 of 40 Pa.[43] For a given surface, $T < T_{eq}$ corresponds to the regime where adsorption is faster than desorption, thus fostering CO_2 capture, whereas for $T > T_{eq}$ the CO_2 desorption would dominate.

Before exploring the *T*-dependent rates as plot in Figure 4, it is worth pointing out that the desorption rates depend on E_{ads}, and this, in turn, is also dependent on the particular DFT method used. Specifically, we already discussed that including dispersion terms, not accounted for in the present work, would lead to stronger E_{ads} values, and could therefore shift to larger T_{eq} values. However, the effect of the DFT method, including the effect of dispersion, will equally affect all the studied systems and, since the relevant comparison is T_{eq} for a given material relative to T_{eq} for stoichiometric TiC (001), which we will denote as T_{eq}^{TiC}, these relative values of T_{eq} are therefore robust to the neglect of dispersion corrections. From Figure 4, one can see that, for the example, for the Sr-doped TiC (001) surface, T_{eq} is 230 K higher than T_{eq}^{TiC}, whereas for In-doped TiC (001), the temperature would be ~80 K lower. In a nutshell, this indicates that doping of metal carbides may broaden the tuning of CO_2 capture, and so can provide a route to further improve their CCS capability.

4. Conclusions

A systematic study of the effect of doping on TiC (001) surface by different representative elements across the periodic table (Mg, Ca, Sr, Al, Ga, In, Si, Sn, Pd, Pt, Rh, Ir, La, and Ce) on CO_2 adsorption has been carried in the framework of DFT. The results show that introduction of dopants replacing one Ti surface atom has significant effects on the CO_2 adsorption properties. In particular, dopants may significantly modify the adsorption energy and, hence, the desorption rate —at a given temperature— which will have an impact on the CCS capability of these materials. Most often, the adsorption energy increases, although it is found to decrease when doping with some *p* block elements such as In and Sn.

The analysis of the results provided some trends that can be used for further screening. Thus, the adsorption energy is reasonable correlated with difference in the net charge of the surface carbon atoms comparing the doped and undoped systems. The surface distortions introduced by the dopant also plays a major role. In this sense, it has been found that the adsorption energy correlates rather well with the difference in the (empirical) atomic radii between the dopant and Ti, ΔR. This finding provides a useful descriptor that allows one to predict the effect on the adsorption energy of other dopants without needing to carry out any DFT calculation. The validity of this descriptor has been confirmed by including the cases of early transition metal atoms studied in a previous work. Finally, note that although the ΔR descriptor has been deduced for TiC (001) it is likely to hold for other transition metal carbides. The final rule of thumb is that the larger the ionic crystal size of the dopant, the larger the CO_2 adsorption energy.

Supporting information

The relevant input and output files corresponding to the optimized geometry for the clean doped surface and for CO_2 chemisorption thereon have been uploaded to the NOMAD repository and can be reached at https://dx.doi.org/10.17172/NOMAD/2020.03.27-1

Additional Supporting Information including the atomic structures and details on PAWs used is available free of charge at DOI:XXXXXX.

Acknowledgments

The research carried out at the *Universitat de Barcelona* has been supported by the Spanish MICIUN/FEDER RTI2018-095460-B-I00 and *María de Maeztu* MDM-2017-0767 grants and, in part, by *Generalitat de Catalunya* 2017SGR13 grant and by the COST Action 18234, supported by COST (European Cooperation in Science and Technology). M. N. acknowledges support from Science Foundation Ireland and the Horizon 2020 M-ERA.net 2 co-fund program, through grant agreements No 685451 and 16/M-ERA/3418, M.L acknowledges the HPC-EUROPA3 (INFRAIA-2016-1-730897) project supported by the EC Research Innovation Action under the H2020 Programme, the Tyndall National Institute and the Irish Centre for High-End Computing (ICHEC) for supporting his stay in Cork. F. V. thanks the Spanish MINECO for postdoctoral contracts under the *Ramón y Cajal* Program (RYC-2012-10129) and F. I. acknowledges additional support from the 2015 ICREA Academia Award for Excellence in University Research.

Table 1. Metallic dopants ionic crystal radii, R_{dop},[a] dopant distances to carbon in the surface plane distance, d(CM), and doping formation energies, ΔE_{dop}, as well as when allowing surface relaxation, ΔE_{dop}^{relax}, and energy difference between subsurface and surface doping, where positive values imply a preference for surface doping, $\Delta E_{sub\text{-}surf}$. Distances and radii are given in Å whereas energies in eV. The Ti^{4+} dopant refers to the pristine, undoped surface, used as a reference.

Dopant	R_{dop}	d**(CM)**	ΔE_{dop}	ΔE_{dop}^{relax}	$\Delta E_{sub-surf}$
Ti^{4+}	0.65	2.17	0	0	0
Mg^{2+}	0.80	2.26	11.42	11.09	0.74
Ca^{2+}	1.14*	2.39	10.86	10.65	1.99
Sr^{2+}	1.32*	2.59	11.64	11.40	1.54
Al^{3+}	0.62	2.19	8.66	8.34	0.39
Ga^{3+}	0.69	2.22	11.03	10.71	0.99
In^{3+}	0.94	2.28	11.85	11.62	1.79
Si^{4+}	0.54*	2.12	8.40	8.20	0.65
Sn^{4+}	0.76	2.26	11.12	10.90	1.45
Rh^{4+}	0.74 *	2.20	6.50	6.17	0.26
Ir^{4+}	0.77*	2.19	4.89	4.54	0.44
Pd^{4+}	0.76*	2.23	9.84	9.53	0.31
Pt^{4+}	0.77*	2.21	7.64	7.30	0.32
La^{3+}	1.18*	2.46	7.14	6.94	4.86
Ce^{4+}	1.01*	2.33	6.02	5.85	3.28

[a] The dopants ionic crystal radii reported were provided by the Atomistic Simulation Group lead by Prof. Robin Grimes at the Imperial College London. These correspond to surface atoms —five-fold coordination— or, when this information is not available, to six-fold coordination, the latter are marked with an asterisk.

Table 2. Bader charges of the dopant, q^{dop}, and on the C atoms surrounding it at the surface, q^{surf}, and just beneath it, q^{sub}. All values are given in *e*.

Dopant	q^{surf}	q^{sub}	q^{dop}
Ti	-1.70	-1.81	+1.81
Mg	-1.71	-1.87	+1.63
Ca	-1.65	-1.74	+1.45
Sr	-1.63	-1.66	+1.40
Al	-1.82	-2.00	+2.23
Ga	-1.61	-1.79	+1.20
In	-1.58	-1.79	+1.20
Si	-1.77	-2.05	+2.32
Sn	-1.63	-1.86	+1.53
Rh	-1.50	-1.53	+0.62
Ir	-1.51	-1.57	+0.80
Pd	-1.48	-1.56	+0.49
Pt	-1.43	-1.52	+0.31
La	-1.65	-1.74	+1.64
Ce	-1.66	-1.76	+1.66

Table 3. Preferred adsorption mode, adsorption energy, E_{ads}, in eV, and structural parameters of CO_2 on the different doped TiC (001) surfaces. The α(OCO) stands for the bond angle of the adsorbed molecule, given in degrees, whereas *d*(CC) and *d*(CO) stand for the distances between the C atom of CO_2 and the closest C atom of the TiC surface —when the two bonds are different, two values are given—, and the average C-O distance in the adsorbed molecule, both in Å. The q_{CO_2} term refers to the Bader charge of the CO_2 molecule, given in *e*.

Dopant	**Mode**	E_{ads}	**α(OCO)**	***d*(CC)**	***d*(CO)**	q_{CO_2}
Ti	TopC	-0.61	127.5	1.48	1.29	-0.82
Mg	TopC-A	-0.77	127.3	1.47	1.29	-0.86
Ca	TopC-A	-1.08	124.1	1.44	1.31	-1.17
Sr	TopC-A	-1.22	121.7	1.43	1.32	-1.28
Al	TopC-A	-0.77	127.7	1.47	1.29	-0.82
Ga	TopC-A	-0.72	128.0	1.48	1.29	-0.83
In	TopC	-0.50	125.4	1.50	1.29	-0.80
Si	TopC-A	-1.02	127.1	1.46	1.29	-0.82
Sn	TopC-A	-0.57	128.2	1.48	1.29	-0.90
Rh	TopC-A	-0.71	128.1	1.49	1.28	-0.76
Ir	TopC-A	-0.62	128.5	1.49	1.28	-0.78
Pd	TopC-A	-0.73	128.2	1.49	1.28	-0.81
Pt	TopC-A	-0.68	128.4	1.49	1.28	-0.79
La	TopC-A	-1.07	123.1	1.44	1.31	-1.25
Ce	TopC	-1.10	123.4	1.52	1.29, 1.30	-0.86

Figure 1. Schematic top view of the MMC, TopC, and TopC-A adsorption modes, where Ti, C, and O atoms are represented by blue, brown, and red spheres, respectively, whereas the dopant is shown in pale grey.

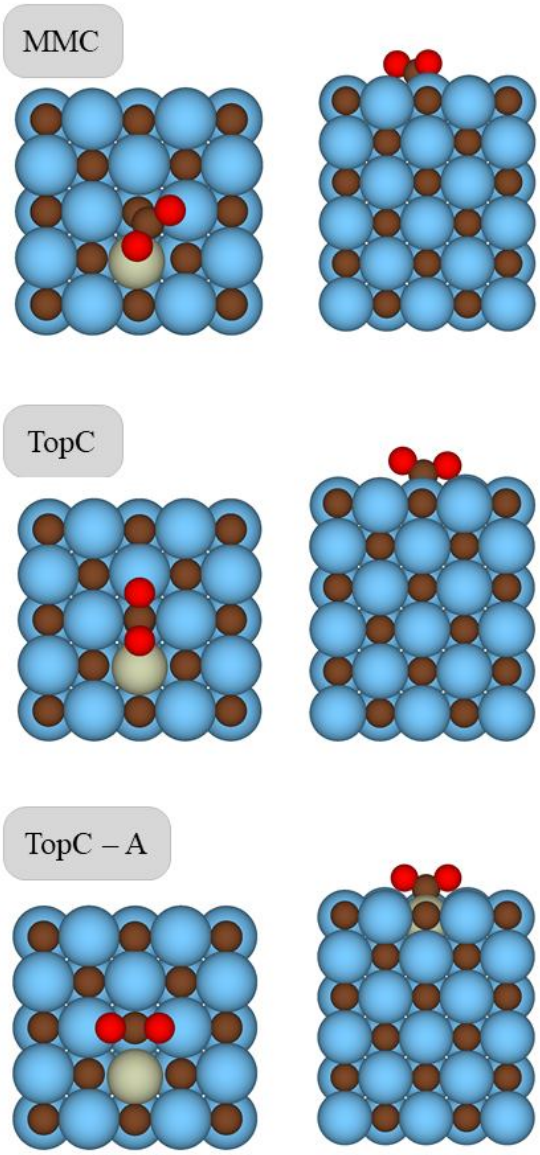

Figure 2. Adsorption energy, E_{ads}, trend *vs.* the difference between the net charge of the surface carbon bonded to CO_2 and net charge of the same carbon for the clean surface, Δq^{surf}, *i.e.* q^{surf} values given in Table 1, plus 1.70 *e* accounting for the clean surface. Each group of explored metals is differentiated by colours, as well as the Ti reference in TiC.

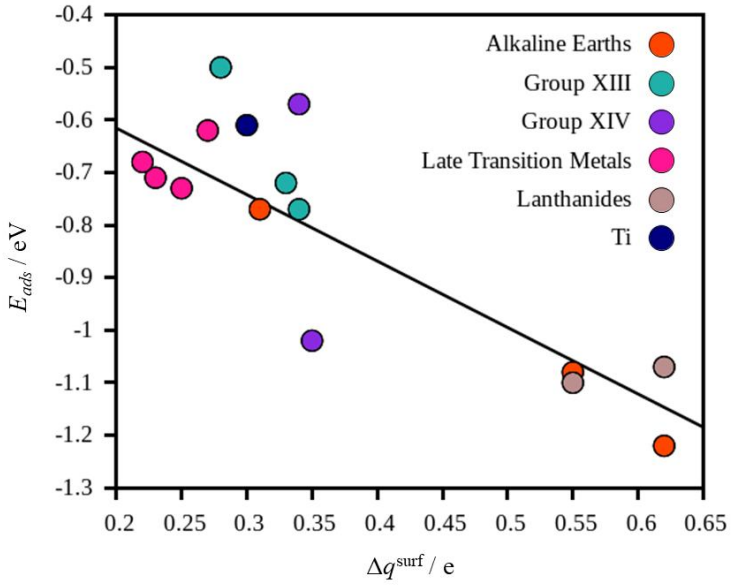

Figure 3. Evolution of the computed adsorption energies, E_{ads}, as a function of the absolute value of ΔR, as defined in Eq. 4. The left panel includes all studied elements, whereas the middle panel shows the improved correlation when neglecting Si and In outliers. Finally, the right panel consider the elements from the middle panel plus all the early transition metals previously studied.[22] Legend is as in Figure 2, except for early transition metals, specified.

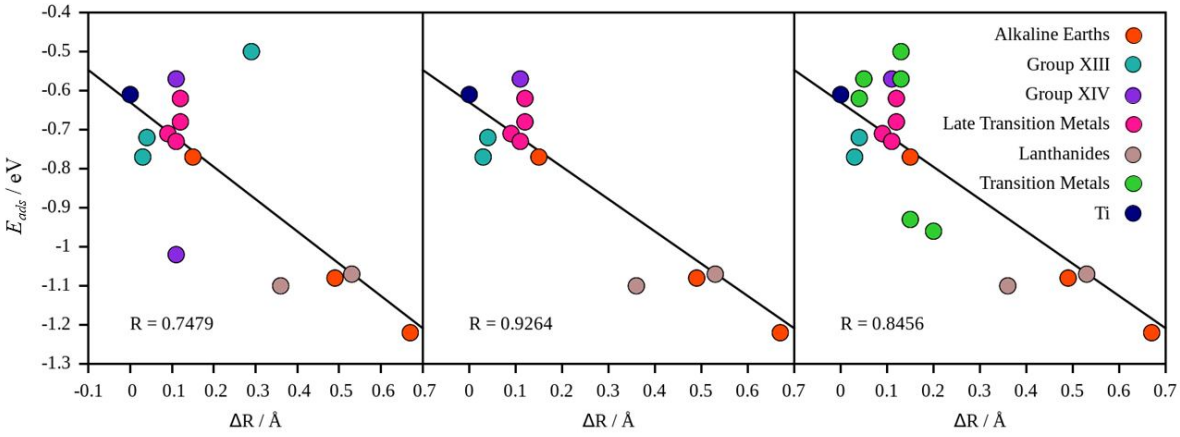

Figure 4. Calculated CO_2 desorption rates, r_{des}, on doped TiC (001) at the current partial pressure of atmospheric CO_2 of 40 Pa. Note that the adsorption rate does not depend on the adsorption energy and, hence, is the same for all cases. The desorption rates of the undoped and doped surfaces are shown color-coded.

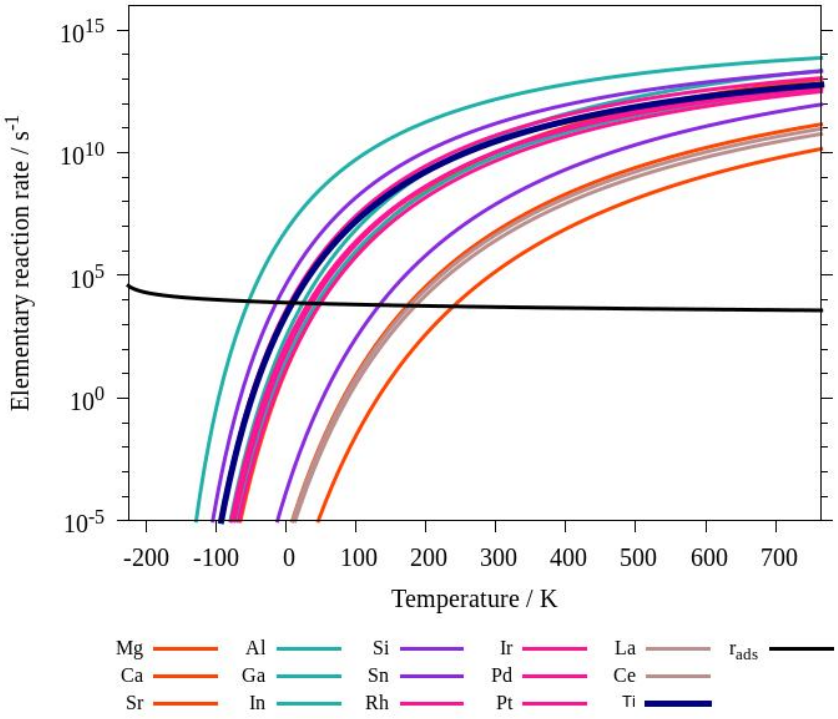

References

(1) Doney, S. C.; Fabry, V. J.; Feely, R. A.; Kleypas, J. A. Ocean Acidification: The Other CO_2 Problem. *Annu. Rev. Mar. Sci.*, **2009**, *1*, 169-192.

(2) Leuliette, E. W.; Willis, J. K. Balancing the Sea Level Budget, *Oceanography*, **2011**, *24*, 122-129.

(3) Cox, P. M.; Betts, R. A.; Jones, C. D,: Spall, S. A,: Totterdell, I. J. Acceleration of Global Warming due to Carbon-Cycle Feedbacks in a Coupled Climate Model. *Nature*, **2000**, *408*, 184-187.

(4) Atabami, A. E.; Silitonga, A. S.; Badruddin, I. A.; Mahlia, T. M. I.; Masjuki, H. H.; Mekhilef, S. A. Comprehensive Review on Biodiesel as an Alternative Energy Source and its Characteristics. *Renew. Sustain. Energy Rev.*, **2012**, *16*, 2070-2093.

(5) Panwar, N.L.; Kaushik, S.C.; Kothari, S. Role of Renewable Energy Sources in Environmental Protection: A Review. *Renew. Sustain. Energy Rev.,* **2011**, *15*, 1513-1524.

(6) Balat, M. Potential Alternatives to Edible Oils for Biodiesel Production – A Review of Current Work. *Energy Convers. Manag.*, **2011**, *52*, 1479-1492.

(7) Espinal, L.; Poster, D. L.; Wong-Ng, W.; Allen, A. J.; Green, M. L. Measurement, Standards, and Data Needs for CO_2 Capture Materials: A Critical Review, *Environ. Sci. Technol.*, **2013**, *47*, 11960 -11975.

(8) D'Alessandro, D. M.; Smit, B.; Long, J. R. Carbon Dioxide Capture: Prospects for New Materials, *Angew. Chem., Int. Ed.*, **2010**, *49*, 6058-6082.

(9) Bui, M.; Adjiman, C. S.; Bardow, A.; Anthony, E. J.; Boston, A.; Brown, S.; Fennell, P. S.; Fuss, S.; Galindo, A.; Hackett, L. A.; *et al*., Carbon Capture and Storage (CCS): the Way Forward, *Energy Environ. Sci.***, 2018**, *11*, 1062-1176.

(10) Markewitz, P.; Kuckshinrichs, W.; Leinter, W.; Linssen, J.; Zapp, P.; Bongartz, R.; Schreiber, A.; Müller, T. E. Worldwide Innovations in the Development of Carbon Capture Technologies and the Utilization of CO_2, *Energy Environ. Sci.*, **2012**, *5*, 7281-7305.

(11) Hessami, M.-A.; Stewart, C. A Study of Methods of Carbon Dioxide Capture and Sequestration - the Sustainability of a Photosynthetic Bioreactor Approach. *Energy Convers. Manag.*, **2005**, *46*, 403-420.

(12) Cheng-Hsiu, Y.; Chihi-Hung, H.; Chung-Sung, T. A Review of CO_2 Capture by Absorption and Adsorption, *Aerosol Air Qual. Res.*, **2016**, *12*, 745 -769.

(13) Fernández-García M, Anderson J. A. Supported Metals in Catalysis, C*atalytic Sciences Series*, V*ol. 5*, **2003**, Imperial College Press, London

(14) Rodriguez, J. A.; Evans, J.; Feria, L,; Vidal, A. B.; Liu, P.; Nakamura, K.; Illas, F. CO_2 Hydrogenation on Au/TiC, Cu/TiC, and Ni/TiC Catalysts: Production of CO, Methanol, and Methane. *J. Catal.*, **2013**, *307*, 162-169.

(15) Vidal, A. B.; Feria, L.; Evans, J.; Takahashi, Y.; Liu, P.; Nakamura, K.; Illas, F.; Rodriguez, J. A. CO_2 Activation and Methanol Synthesis on Novel Au/TiC and Cu/TiC Catalysts. *J. Phys. Chem. Lett.*, **2012**, *3*, 2275–2280.

(16) Posada-Pérez, S.; Viñes, F.; Ramirez, P. J.; Vidal, A. B.; Rodriguez, J. A.; Illas, F. The Bending Machine: CO_2 Activation and Hydrogenation on δ-MoC(001) and β-Mo_2C(001) Surfaces. *Phys. Chem. Chem. Phys.* **2014**, *16*, 14912–14921.

(17) Liu, X.; Kunkel, C.; Ramírez de la Piscina, P.; Homs, N.; Viñes, F.; Illas, F. Effective and Highly Selective CO Generation from CO_2 Using a Polycrystalline α-Mo_2C Catalyst. *ACS Catal.* **2017**, *7*, 4323-4335.

(18) Kunkel, C.; Viñes, F.; Illas, F. Transition Metal Carbides as Novel Materials for CO_2 Capture, Storage, and Activation. *Energy Environ. Sci.* **2016**, *9*, 141–144.

(19) Porosoff, M. D.; Kattel, S.; Li, W.; Liu, P.; Chen, J. G. Identifying Trends and Descriptors for Selective CO_2 Conversion to CO over Transition Metal Carbides. *Chem. Commun.* **2015**, *51*, 6988–6991.

(20) Porosoff, M. D.; Yang, X.; Boscoboinik, J. A.; Chen, J. G. Molybdenum Carbide as Alternative Catalysts to Precious Metals for Highly Selective Reduction of CO_2 to CO, *Angew. Chem., Int. Ed.*, **2014**, *53*, 6705 - 6709.

(21) Schweitzer, N. M.; Schaidle, J. A.; Ezekoye, O. K.; Pan, X.; Linic, S.; Thompson, L. T. High Activity Carbide Supported Catalysts for Water Gas Shift, *J. Am. Chem. Soc.*, **2011**, *133*, 2378 - 2381.

(22) López, M.; Broderick, L.; Carey, J. J.; Viñes, F.; Nolan, M.; Illas, F. Tuning Transition Metal Carbide Activity by Surface Metal Alloying: a Case Study on CO_2 Capture and Activation, *Phys. Chem. Chem. Phys.*, **2018**, *20*, 22179-22186.

(23) Yerskin, I.; Nolan, M. Doping of Ceria Surfaces with Lantanium: a DFT +U Study. *J. Phys. Condens. Matter*. **2010**, *22*, 135004.

(24) Nolan, M. Enhanced Oxygen Vacancy Formation in Ceria (111) and (100) Surfaces Doped with Divalent Cations. *J. Mater. Chem.* **2011**, *21*, 9160–9168.

(25) Perdew, J. P.; Burke, K.; Ernzerhof, M. Generalized Gradient Approximation Made Simple. *Phys. Rev. Lett.* **1996**, *77*, 3865–3868.

(26) Quesne, M. G.; Roldán, A.; Leeuw, N. H.; Catlow, C. R. A.; Bulk and Surface Properties of Metal Carbides: Implications for Catalysis. *Phys. Chem. Chem. Phys.* **2018**, *20*, 6905-6916.

(27) Politi, J. d. S. R.; Viñes, F.; Rodriguez, J. A.; Illas, F. Atomic and Electronic Structure of Molybdenum Carbide Phases: Bulk and Low Miller-Index Surfaces. *Phys. Chem. Chem. Phys.* **2013**, *15*, 12617-12625.

(28) Ahuja, R.; Eriksson, O.; Wills, J. M.; Johansson B. Structural, Elastic, and High-Pressure Properties of Cubic TiC, TiN, and TiO. *Phys. Rev. B* **1996**, *53*, 3072-3079.

(29) Viñes, F.; Sousa, C.; Liu, P.; Rodriguez, J.A.; Illas F. A Systematic Density Functional Theory Study of the Electronic Structure of Bulk and (001) Surface of Transition-Metals Carbides. *J. Chem. Phys.* **2005**, *122*, 174709.

(30) Perdew, J.; Chevary, J. A.; Vosko, S. H.; Jackson, K. A.; Pederson, M. R.; Singh, D. J.; Fiolhais, C. Atoms, Molecules, Solids, and Surfaces: Applications of the Generalized Gradient Approximation for Exchange and Correlation. *Phys. Rev. B* **1992**, *46*, 6671-6687.

(31) Hammer, B.; Hansen, L. B.; Nørskov, J. K. Improved Adsorption Energetics within Density-Functional Theory Using Revised Perdew-Burke-Ernzerhof Functionals. *Phys. Rev. B* **1999**, *59*, 7413-7421.

(32) Kunkel, C.; Viñes, F.; Ramírez, P. J.; Rodriguez, J. A.; Illas, F. Combining Theory and Experiment for Multitechnique Characterization of Activated CO_2 on Transition Metal Carbide (001) Surfaces. *J. Phys. Chem. C* **2019**, *123*, 7567-7576.

(33) Vogiatzis D. K.; Mavrandonakis, A.; Klopper, W.; Froudakis, G. E. Ab initio Study of the Interactions between CO_2 and N-Containing Organic Heterocycles. C*hemPhysChem*, **2009**, *10*, 374-383.

(34) Bader, R. F. W. Atoms in Molecules: A Quantum Theory, International Series of Monographs on Chemistry, ISBN-10: 0198558651, Clarendon Press; Oxford, United Kingdom, New Ed. 1994.

(35) Kresse, G.; Furthmüller, J. Efficiency of *Ab-initio* Total Energy Calculations for Metals and Semiconductors Using a Plane-Wave Basis Set. *Comput. Mat. Sci.* **1996**, 6, 15-50.

(36) Kresse, G.; Furthmüller, J. Efficient Iterative Schemes for Ab Initio Total-Energy Calculations Using a Plane-Wave Basis Set. *Phys. Rev. B* **1996**, *54*, 11169–11186.

(37) Kresse, G.; Joubert, D. From Ultrasoft Pseudopotentials to the Projector Augmented-Wave Method. *Phys. Rev. B* **1999**, *59*, 1758–1775.

(38) Blöchl, P. E. Projector Augmented-Wave Method. *Phys. Rev. B* **1994**, *50*, 17953–17979.

(39) Monkhorst, H. J.; Pack, J. D. Special Points for Brillouin-Zone Integrations. *Phys. Rev. B* **1976**, *13*, 5188–5192.

(40) Ham, D. J.; Lee, J. S. Transition Metal Carbides and Nitrides as Electrode Materials for Low Temperature Fuel Cells. *Energies* **2009**, *2*, 873-899.

(41) Cordero, B.; Gómez, V.; Platero-Prats, A. E.; Revés, M.; Echevarría, J.; Cremades, E.; Álvarez, S. Covalent Radii Revisited. *Dalton Trans.*, **2008**, *21*, 2832-2838.

(42) Chen, K. Y.; Kamran, S. Bonding Characteristics of TiC and TiN. *Model. Simul. Mater. Sci.*, **2013**, *3*, 7-11.

(43) Takahashi, T.; Sutherland, S.; Kozyr, A. Global Ocean Surface Water Partial Pressure of CO_2 Database: Measurements Performed During 1957–2014 (Version 2014). *Environmental Sciences Division*, **2015**, Oak Ridge National Laboratory.

Table of Contents Graphic